Quantitative Calculation of Aquifer Water Quantity Using TEM Data

Lanying Huang[1], Shengdong Liu[1], Bo Wang[1*], Fubao Zhou[2]

1 State Key Laboratory of Deep Geomechanics & Underground Engineering and School of Resource and Earth Science,
China University of Mining and Technology, Xuzhou 221116, China
2 School of Safety Engineering, China University of Mining and Technology, Xuzhou 221116, China

Email of Corresponding Author: wbsyes@126.com

ABSTRACT

Mine water is a menace to coal mining. Mine water quantity is detected by drilling in the coal mine roadway, and the disadvantage is the high workload and low efficiency. Therefore, transient electromagnetic method (TEM) was proposed, and TEM data was processed to detect the water yield property of a targeted layer in the coal mine. Through a mine-oriented 3D Transient Electromagnetic Method observing system, the signal of induced voltage is obtainable. Transient Electromagnetic Method 3D data volume can be calculated through the calculation of all-time resistivity and time-depth conversion. After an appropriate apparent resistivity value is set, the spatial distribution range of an aquifer can be determined. Then, with the water-filling coefficient of the aquifer, its water quantity can be estimated. The water yield property detection results in the No.4 coal seam goaf of the No.80101 workface in Jude Mine of Shanxi, China, demonstrates that the apparent resistivity of this goaf is less than 3 Ω.m, and the projection area of low resistivity anomaly zone is 22,383 m^2. By using the formula Q=KMS, we can estimate that the water volume is 33,574 m^3. Three boreholes have been constructed for the next dredging and drainage project, which results in a total water yield of 33,089 m^3. The error percentage of the predicted water quantity is less than 1.5%. It can thus be concluded that it is feasible to predict aquifer water content with TEM data.

Cálculo cuantitativo del volumen de aguas subterráneas a través del Método Electromagnético Transitorio (TEM)

RESUMEN

El agua al interior de las minas es una amenaza para la minería de carbón. La cantidad del agua en las minas se detecta al perforar en las vías del socavón, con la desventaja de la carga de trabajo y la baja eficacia que significan. Por esto, el presente trabajo propone el Método Electromagnético Transitorio (TEM, del inglés Transient Electromagnetic Method) y utiliza la información generada para detectar las propiedades de producción de agua en una capa específica de una mina de carbón. A través de un sistema de observación tridimensional TEM orientado a minas se puede obtener la señal del voltaje inducido. La capacidad de la información del sistema TEM tridimensional se puede calcular al obtener la resistividad y la conversión tiempo-profundidad. Tan pronto se establece el valor apropiado de la resistividad aparente se puede determinar el rango de distribución de un acuífero. Luego, con el coeficiente de saturación del acuífero se puede calcular la cantidad de agua. Los resultados de la detección de las propiedades de producción de agua en la mina abandonada número cuatro de frente de trabajo número 80101 de la mina Jude, en Shanxi, China, demostró que la resistividad aparente de esta excavación es de 3 Ω.m, y el área de proyección de la zona anómala de baja resistividad es 22.383 m^2. Al usar la fórmula Q=KMS, se estimó que el volumen de agua es de 33,574 m^3. Tres pozos se han construido para el próximo proyecto de dragado y drenaje, cuyos resultados de producción de agua es de 33,089 m^3. El porcentaje de error de la predicción de la cantidad de agua es menor al 1.5 %. Se concluye, por ende, que es factible producir el contenido de agua de un acuífero con la información del TEM.

1. Introduction

China is the largest producer of coal in the world because coal plays an essential role in the economic development of China (Figure 1). Coal mining accidents have become a frequent occurrence in recent years (Zhang et al., 2014; Wang et al., 2016). Although the death rate resulting from these accidents in China has declined, it is still 70 times higher than that in the United States and 17 times higher than that in South Africa. Against this backdrop, it is urgent to study how to find effective ways to detect water quantity in the aquifer and reduce coal mining accidents (Zhang et al., 2015). Among some geophysical methods currently available, TEM technology is one that has received much attention and has been widely used to reduce coal mining accidents.
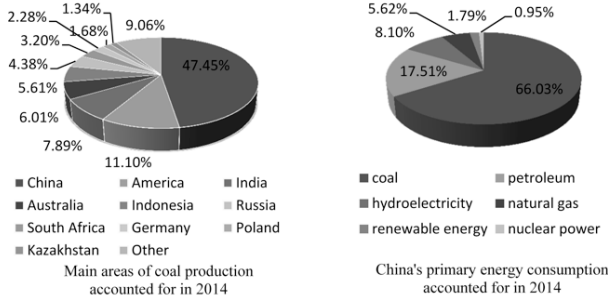

Figure 1. Global coal production structure and energy consumption ratio in China.

In a TEM application, an ungrounded loop-line first transmits downward a pulse-type primary field, which induces an eddy current. The spatial and temporal distribution of a secondary field caused by the eddy current can then be observed through the coil (Yu, 2007; Wang et al., 2011; Tanaka and Kunisada 2011). By measuring the variation rule of the secondary magnetic field over time during the time-off period, the geoelectricity features at different depths can be obtained (Guillemoteau et al., 2011; Tuncer et al., 2014). From Figure 2 it can be seen that TEM receives induced signals during the time-off period, which will be attenuated over time.

By using the TEM method, we can solve some geological problems (Cheng et al., 2013; Hu et al., 2013). Due to its features such as light equipment, little lateral influence, and high resolution, TEM can be widely applied in water disaster prevention and control (Zhang et al., 2010; Mollidor et al., 2013; Xue et al., 2013; Tao et al., 2013). However, because of the focus on theory development and processing method restraints, past analyses have usually been qualitative, which cannot meet the standard of quantification, and, to certain extent, hinders the application of TEM on a wider basis(Xu et al., 2012; Wang et al., 2014). Hence, in this study, we will develop a theory and propose a method to calculate TEM responses. To do so, we will use equivalent substitution, interpret the diffusion law of TEM field from the perspective of physics, calculate physical parameters, and conduct 3D apparent resistivity imaging and quantitative analyses of detection results.
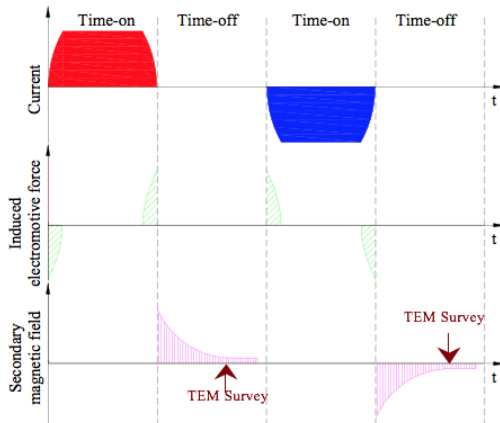

Figure 2 Schematic diagram of TEM survey.

2. TEM Data Processing

2.1. Apparent Resistivity Calculation

The transmitting loop center induction electromotive force $\varepsilon(t)$ of horizontal round loop in uniformity whole space medium is:

$$\varepsilon(t) = \frac{\mu_0 nIS}{\sqrt{\pi} r_0 t} f(u) \tag{1}$$

$$f(u) = u^3 e^{-u^2} \tag{2}$$

$$u = \frac{r_0}{\sqrt{\pi}} \sqrt{\frac{\mu_0}{\rho t}} \tag{3}$$

Where μ_0 is the vacuum permeability, n is the turn number of transmitting loop, I is the respective emission current, S is the receiving loop similar area, r_0 is the transmitting loop radius, t is the observation time and ρ is the true resistivity of the medium.

From Equation (3), we can obtain an equation as below:

$$\rho_s^{all} = \mu_0 r_0^2 / (\pi t u^2) \tag{4}$$

If the loop forms a square about b meters on a side, and $r_0 = b/\sqrt{\pi}$, then, with Equations (1) ~ (4), the all-time apparent resistivity ρ_s^{all} can be calculated with the binary search algorithm. The calculation process is illustrated in Figure 3.

For any observation window t, u is set as $[0,10]$, and the searching region of u can be seen as an absolute value, and among them, u_s is the initial value of the searching region, u_e is final value, u_e is a median value which is u value. u is calculated by a binary search algorithm. is actual measured magnetic value, and $H(t_i)$ is:

$$H_1(t) = \frac{\sqrt{\pi} NIt}{4at_0} \left[2u^2 + (1-2u^2)\varphi(u) - \frac{2}{\sqrt{\pi}} ue^{-u^2} \right] \quad 0 < t < t_0 \tag{5}$$

$$H_2(t) = \frac{\sqrt{\pi} NIt}{4at_0} (1-2u^2)\varphi(u) - \frac{NIt}{2at_0} ue^{-u^2}$$
$$+ \frac{\sqrt{\pi} NI}{4a} \left(1 + \frac{2t}{t_0} u^2 - \frac{t}{t_0}\right) \varphi\left(u/\sqrt{1-t_0/t}\right) \quad t > t_0 \tag{6}$$
$$+ \frac{NI}{2a\sqrt{1-t_0/t}} \left(\frac{t}{t_0} - 1\right) ue^{-u^2/(1-t_0/t)}$$

2.2. Depth Conversion

The detection depth D of the TEM method is related to transmitting magnetic torque, all-time apparent resistivity, and the minimum resolutive voltage. The time-depth conversion equation for mine-oriented TEM method is:

$$V_s = \alpha \frac{\rho_s^{all} \sqrt{\gamma\pi}}{\mu\alpha} \{C_1 + (C_1^2)^{1/2} + [1 + \frac{C_1}{(C_1^2+2)^{1/2}}]\gamma C_2\} \tag{7}$$

$$D = V_S \times t_i \tag{8}$$

$$C_1(\gamma) = \frac{3\sqrt{\pi}}{4} [1 - \frac{\gamma}{4} - \sum_{k=1}^{\infty} \frac{(2k-3)!!}{k!(k+1)!} (\frac{\gamma}{2})^k] \tag{9}$$

$$C_2(\gamma) = \frac{3\sqrt{\pi}}{4} [1 - \frac{\gamma}{4} - \sum_{k=0}^{\infty} \frac{(2k-1)!!}{k!(k+1)!} (\frac{\gamma}{2})^k] \tag{10}$$

where α is the conversion coefficient, which is about the heterogeneous conductor in the vicinity of the roadway and usually values between 0.6 and 1.8; β is the factor of proportionality and $\gamma = \mu\alpha^2/(4\rho_i t_i)$, where ρ_i is the corresponding resistivity value of moment t_i.
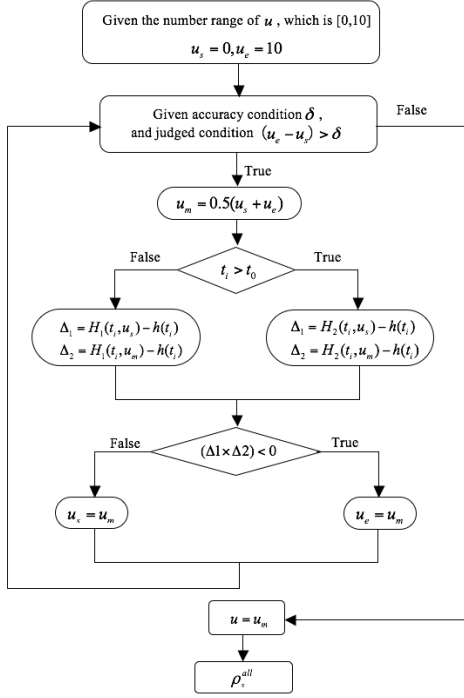

Figure 3. The solving procedure of apparent resistivity.

2.3. Interpolation Operation

Due to the unstable workload, the measured and computational data of experiment and field are always not accurate enough, so interpolation is introduced as a supplement.

$K(x_k, y_k, z_k)$ is an arbitrary point in the three-dimensional space. There is given point $J(x_i, y_i, z_i), i = 1,2,3,\cdots,n$, which is the vicinity of K. The inverse distance weighting method can be used to attribute the value

$$X_K = \frac{\sum\limits_{i=1}^{n} \dfrac{x_i}{d_i^2}}{\sum\limits_{i=1}^{n} \dfrac{1}{d_i^2}} \tag{11}$$

X_K with the equation:

Where d_i is the distance between the interpolating point and the given point in the vicinity. Y_K and Z_K can be calculated in the same way as X_K.

2.3. 3D Slice Extraction

3D visualization is a technique to reveal and describe spatial data, receive the subsurface geological structure and features, which provides information for accurate description of the 3D geological structure, and facilitate the exploration and development of coal mine.

According to the data received from different detection directions, it can be seen that 3D visualization can clearly display the spatial distribution of anomalies with different resistivity values that correspond to different threshold values, the scattered points, and the range of apparent resistivity. However, a cross-section map can be clearer in showing the anomaly areas

at a particular depth on a profile. Cross-sections can be extracted from different depths of Plane XY, YZ, and ZX. Apparent resistivity data can be extracted from any depth or vertical profile.

2.4. Aquifer Water Quantity Estimation

Through the cross-section map, the aquifer water volume can be calculated with the following formula:

$$Q = K \times M \times S$$

$$(12)$$

In this equation, Q is the aquifer water quantity, K is the water containing coefficient, M is the aquifer thickness, and S is the water-rich area in the aquifer.

3. Field Application

3.1. Geological Setting

The No.80101 Workface of Jude Mine in Shanxi Province is under L1 limestone in the middle and lower part of Taiyuan formation, 60.6m beneath the 4# seam. The seam occurrence is stable with a thickness range of 1.8 to 3.2m, and a 2.8m thickness on average. Part of the area contains a 0.05 to 0.1m dirt band of mudstone or carbonolite (carbonaceous mudstone). At the bottom of the seam is a pyrite seam in forms of lamella and nodule. The lithological column is shown in Figure 4.

3.2. Field Detection

To detect the spatial distribution of the goaf and estimate the water quantity, MTEM was adopted with the YCS360 Electromagnetic System (as shown in Figure 5). The detection of the No.80101 workface starts at the intersection of the return airway and the concentrated rail roadway, then goes on from the return airway to the openoff cut, and ends at the intersection of intake airway and concentrated rail roadway. The total detection workload is 3470 m, including 1660 m along the return airway, 150 m in the openoff cut, and 1660 m along the intake airway. Monitoring points are set every 10 meters, and the detection is conducted in 6 directions, including 60°, 45°, and 30° to the external wall roof, standard to the ceiling, and 30° and 45° to the interior wall roof. The TEM detection direction diagram is shown

Figure 4. Lithological column.

Table 1. Drilling log table of anomaly YC7 in No.80101 workface

Location	Drilling Log Number	Parameter			Final Hole Position	Hydrology	Source	Total Volume (m³)
		Azimuth (°)	Dip (°)	Depth (m)				
	H19-1	313	37	129	115m to 4# seam	water yield 8m³/h at 60m	limestone water above 8# seam	3,685
	H19-2	277	46	125	90m to 4# goaf	water yield 30m³/h from final hole	goaf water from 4# seam	15,267
No.18 drilling field of No.80101 return airway	H19-3	221	41	130	95m to 4# goaf	water yield 35m³/h from final hole	goaf water from 4# seam	12,379
	H19-4	136	36	157	99m to 4# goaf	none	/	/
	H19-5	237	-1	141	Floor of 8# seam	none	/	/
	H19-6	221	1	132	Floor of 8# seam	none	/	/
	H19-7	229	-10	130	Floor of 8# seam	none	/	/
	H19-S1	238	35	111	4# seam	water yield 3m³/h from final hole	goaf water from 4# seam	5,443
	H19-S2	308	30	156	109m to 4# goaf	none	/	/

6.50	46.87	L5 limestone
1.50	48.37	Mudstone
0.50	48.87	Upper-6 seam
1.00	49.87	Mudstone
0.40	50.27	Lower-6 seam
3.50	53.77	Sandy mudstone
7.00	62.77	L4 limestone
5.00	65.77	Sandy mudstone
0.50	66.27	7 seam
3.80	70.07	Mudstone
4.50	74.57	Fine sandstone
2.00	76.57	Mudstone

Figure 4. Lithological column.

in Figure 6, and the arrangement diagram of MTEM is shown in Figure 7.

3.3. Data Interpretation and Result Analysis

The data is processed based on the standard flow chart (Figure 8), and data interpretation is carried out from the perspective of geophysical characteristics. The features are shown in 3D images. Water quantity is higher in areas where the fractures are concentrated, indicated by higher electrical conductivity and lower resistivity (i.e., high potentiallow resistivity) anomalies. This characteristic identifies aquifer areas as those where roof resistivity is less than $3\Omega.m$.

Figure 9 is a 3D spatial distribution graph of anomalies at different depths above the No.80101 workface. 40 meters above the roof is a water-rich stratum, and key preventions should be focused on Region YC1, YC7, and YC10. Anomaly area YC7 is located between 1085m and 1850 m along the return airway (between monitoring point KF13 to KF15), 0-120m along the inclination slope (120m within return airway and workface), and 40m to 60m above the roof (more details in Fig 9), with an anomaly-impacted area of 22,383 m2. The goaf water-filling coefficient is 0.25 to 0.35, and the detection result of the actual ratio is 0.3. It is indicated by the effect sketch that M is 5m, based on the equation Q=KMS. Thus we can deduce that Q=33,574m³. The verification of the calculated values based on field measurements is shown in Table 1. H19-2, H19-3 and H19-S1 boreholes have been constructed for the later next and drainage project, which results in a total water quantity of 33,089m3, and the error percentage of the predicted water volume is less than 1.5%.

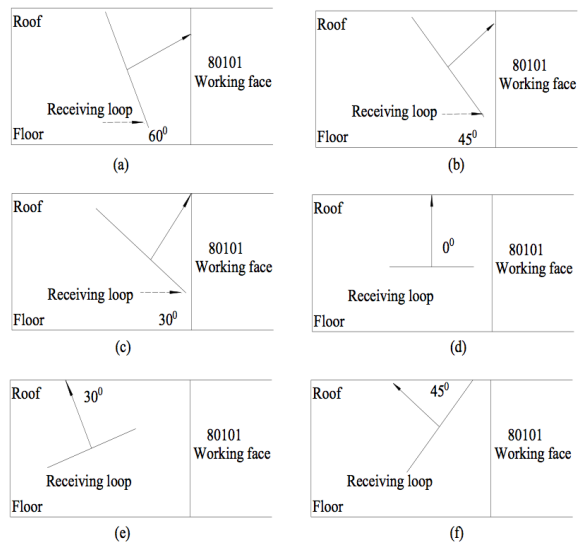**Figure 5.** YCS360 electromagnetic system.

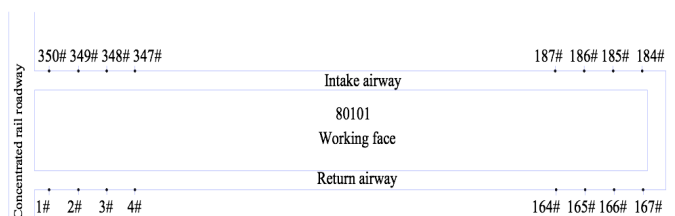**Figure 6.** TEM detection direction diagram.

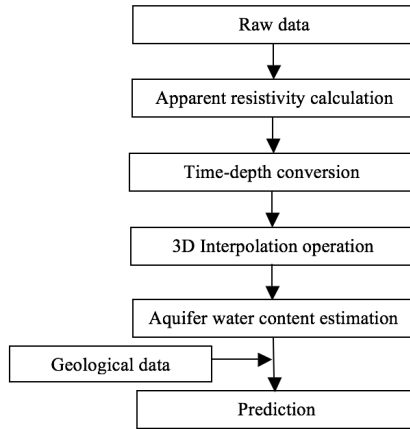**Figure 7.** Arrangement diagram of MTEM.
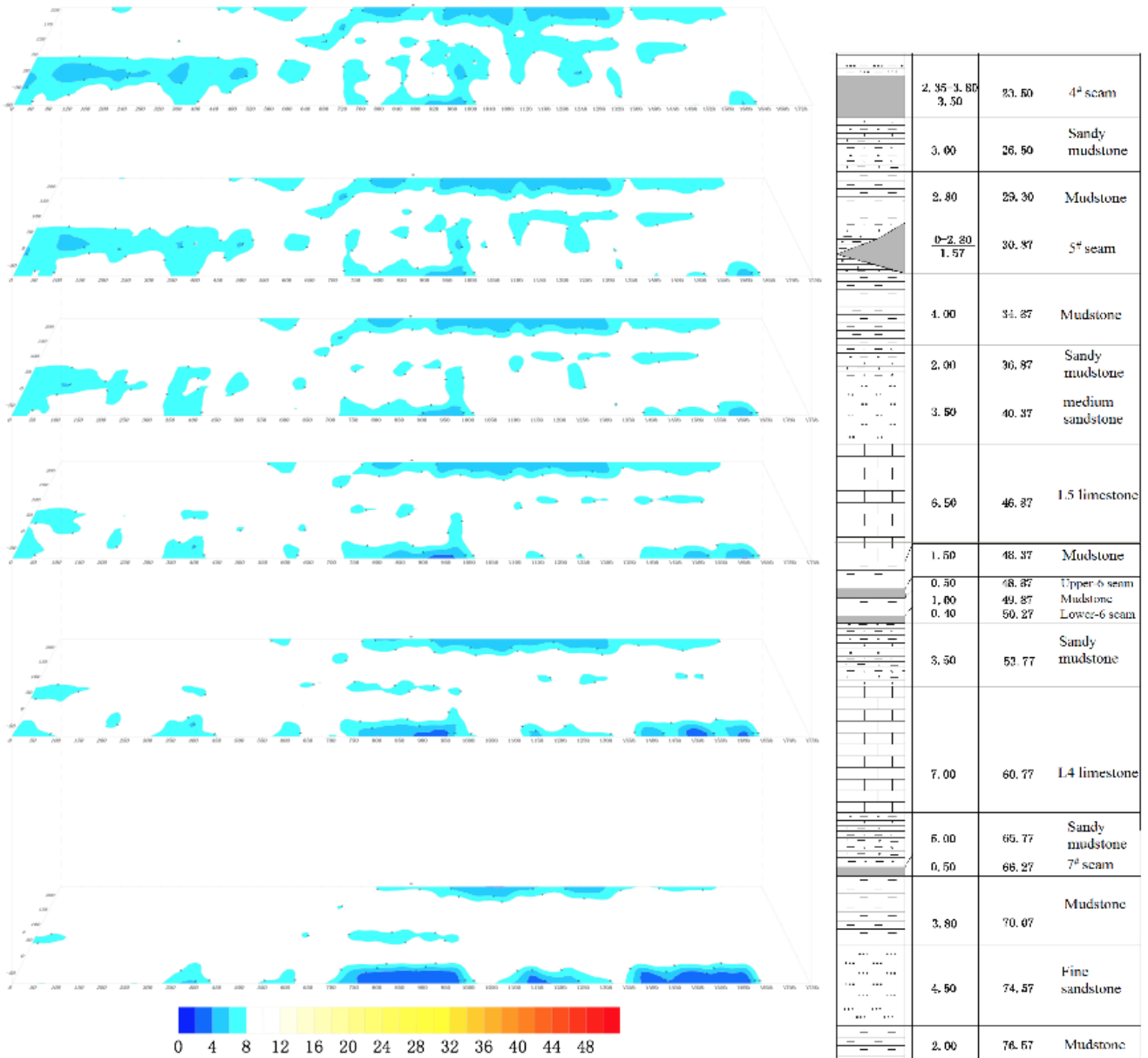
Figure 8. Processing flow chart

Figure 9. The 3D spatial distribution of anomalies at different depths above the No.80101 workface.

4. Conclusions

TEM resistivity imaging boasts rapid imaging, high quantification level, and high resolution, especially when it comes to detecting low resistivity body with a high-resistivity overlayer. With the projection area S of low-resistivity anomaly zone, the water containing coefficient K and the aquifer thickness M, the aquifer water quantity can be estimated with an error percentage of the predicted water quantity below 2%. The TEM 3D presentation and analysis has offered a new method to determine the water amount in an aquifer.

References

Cheng, J. L., Qiu, H., Ye, Y. T., Yan, G. C., Zhou, J., Cheng, F. B., & Zhang, S. S. (2013). Research on wave-field transformation and data processing of the mine Transient Electromagnetic Method. Journal of the China Coal Society, 38(9), 1646-1650.

Guillemoteau, J., Sailhac, P. & Béhaegel, M. (2011). Regularization strategy for the layered Inversion of airborne transient electromagnetic data: application to in-loop data acquired over the basin of Franceville (Gabon). Geophysical Prospecting. Journal of Immunoassay, 59(6), 1132-1143.

Hu, X. W., Zhang, P. S., Cheng, H., Wu, R. X., & Guo, L. Q. (2013). Quantitative assessment of interference induced by roof bolt during advanced detection with Transient Electromagnetic Method in mine. Journal of Rock Mechanics and Engineering, 32, 3275-3282.

Lin, Z., Ge, S., Li, D., & Peng, W. (2015). Structure Characteristics of Acidic Pretreated Fiber and Self-bind Bio-boards for Public Health. Journal of Pure and Applied Microbiology 9, 221-226.

Liu, Z. L. (2014). The groundwater pollution and environmental protection in China. Biotechnology: An Indian Journal, 10, 1883-14886.

Liu, Z. X., Liu, X. C., & Liu, Y.G. (2009). Research on Transient Electromagnetic Field of mine water-bearing structure by physical model experiment. Journal of Rock Mechanics and Engineering, 28(2), 259-266.

Mollidor, L., Tezkan, B., Bergers, R., & Löhken, J. (2013). Float-transient Electromagnetic Method: in-loop transient electromagnetic measurements on Lake Holzmaar, Germany. Geophysical Prospecting, 61(5), 1056-1064.

Tao, F., Li, W. G., Wang, P., & An, S.P. (2013). Research on fine interpretation for water containment of coal mine rock strata by MT imitated TEM depth inversion method. Journal of the China Coal Society, 38(z1), 129-135.

Tanaka, Y., & Kunisada, E. (2011). Study on meshless method using RPIM for Transient Electromagnetic Field. IEEE Transactions on Magnetics, 47(5), 1178-1181.

Tuncer, O., Shanker, B., & Kempel, L. C. (2014). A hybrid vector generalized finite-element method for Transient Electromagnetic Simulations. Electromagnetics, 34 (3-4), 286-297.

Wang, B., Liu, S. D., Liu, J., Huang, L. Y., & Zhao, L. G. (2011). Advanced prediction for multiple disaster sources of laneway under complicated geological conditions. International Journal of Mining Science and Technology, 21, 749-754.

Wang, B., Liu, S. D., Lu, T., & Sun, H. L. (2014). Coal seam thickness detection in mine roadway by using advanced prediction method. Electronic Journal of Geotechnical Engineering, 19, 4753-4762.

Wang, B., Liu, S. D., Zhou, F. B., Lu, T., Huang, L. Y., & Gao, Y. J. (2016). Polarization migration of three-component reflected waves under small migration aperture condition. Acta Geodynamica Et Geomaterialia, 13(1), 1-12.

Xue, G. Q., Cheng, J. L., Zhou, N. N., Chen, W. Y., & Li, H. (2013). Detection and monitoring of water-filled voids using Transient Electromagnetic Method: A case study in Shanxi, China. Environmental Earth Sciences, 70(5), 2263-2270.

Xu, J. P., Liu, S. D., & Wang, B. (2012). Electrical monitoring criterion for water flow in faults activated by mining. Mine Water and the Environment, 31(31), 172-179.

Yu, J. C. (2007). Mine Transient Electromagnetism Prospecting. China University of Mining and Technology Press, Xuzhou.

Zhang, S. F., Meng, L. S., & Du, X. J. (2010). Transient Electromagnetic Method to investigating potential safety hazard of mine-out area in Tailings Pond of a gold mine. Journal of Jilin University (Earth Science Edition), 40(5), 1177-1182.

Zhang, W., Zhang, D. S., Wang, H. Z., & Cheng, J. X. (2015). Comprehensive technical support for high-quality anthracite production: A case study in the Xinqiao coal mine, Yongxia mining Area, China. Minerals, 5(4), 919-935.

Zhang, W., Zhang, D. S., Wu L. X., & Wang H. Z. (2014). On-site radon detection of mining-induced fractures from overlying strata to the surface: a case study of the Baoshan Coal Mine in China. Energies, 7(12), 8483-8507.